D.V. Bandourin, V.F. Konoplyanikov, N.B. Skachkov

Jet energy scale setting with "$\gamma + Jet$" events at LHC energies. Event rates, P_t structure of jet.

1. INTRODUCTION

In this paper we continue the study of "$\gamma + Jet$" process, started in [1] aimed at jet energy scale setting and hadron calorimeter calibration at LHC energies.

This article is organized in the following way. In Section 2 we shall estimate the event number distribution dependence on a value of "back-to-back" $\phi_{(\gamma,jet)}$ angle between the direct photon $\vec{P_t}^{\gamma}$ and jet $\vec{P_t}^{Jet}$ and on the P_t of the initial state radiation (ISR), i.e. ${P_t}^{ISR}$ value. ${P_t}^{\gamma}$ and η^{γ} dependence of rates is also studied in this section. Estimation of "$\gamma + Jet$" event rates for Barrel (HB), Endcap (HE) and Forward (HF) parts of hadron calorimeter (HCAL) is performed in the last subsection of Section 2. In Section 3 we consider the "$\gamma + Jet$" event features in HB region. In particular, we study the P_{tCUT}^{clust} parameter influence on the selection of events with a good photon and jet P_t balance and also the problem of selection of events with suppressed ISR activity. The next subsections are devoted to the P_t structure of jets in $\eta - \phi$ space and to the particles P_t distribution inside and beyond the jet.

2. EVENT RATES FOR DIFFERENT ${P_t}^{\gamma}$ AND η^{γ} INTERVALS.

2.1 Event number distribution dependence on "back-to-back" $\phi_{(\gamma,jet)}$ angle and on ${P_t}^{ISR}$ values.

The definitions of observable physical variables introduced in Section 3.2 of [1] allow us to make the first step in the study of a possible way to select the events with a good ${P_t}^{\gamma}$ and ${P_t}^{Jet}$ balance. Here we shall study the spectrum of P_t56 variable (that is proportional to ${P_t}^{ISR}$ up to the value of intrinsic parton transverse momentum inside a proton) in signal events with direct photons and this spectrum dependence on some of experimentally measurable variables. For this reason the results of 10^7 "$\gamma + Jet$" events generation for every of four ${P_t}^{\gamma}$ intervals (40–50, 100–120, 200–240, 300–360 GeV/c) by use of PYTHIA with account of 2 QCD subprocesses $q\bar{q} \to g + \gamma$ and $q\,g \to q + \gamma$ were analyzed. For this analysis the observables and the "Selection 1" cuts (1–7), defined in Sections 3.2 of [1], with the following cut parameters:

$$P_{tCUT}^{isol} = 5\ GeV/c; \quad \epsilon_{CUT}^{\gamma} = 7\%; \quad \Delta\phi < 15^{\circ}; \quad P_{tCUT}^{clust} = 20\ GeV/c. \tag{1}$$

were used. The value of the luminosity was taken to be $L = 10^{33}\, cm^2 sec^{-1}$ (low LHC luminosity).

In Tables 1, 2 and 4, 5 we present P_t56 spectra for two most illustrative cases of ${P_t}^{\gamma}$ intervals: $40 < {P_t}^{\gamma} < 50\ GeV/c$ (Table 1 and 2) and $200 < {P_t}^{\gamma} < 240\ GeV/c$ (Table 4 and 5). The distributions of the number of events for integrated luminosity $L_{int} = 3\, fb^{-1}$ in different intervals of P_t56 ($\langle k_T \rangle$ was taken to be fixed at PYTHIA default value, i.e. $\langle k_T \rangle = 0.44\, GeV/c$) and for different "back-to-back" angle intervals $\phi_{(\gamma,jet)} = 180^{\circ} \pm \Delta\phi$ ($\Delta\phi = 15^{\circ}$, 10° and 5° as well as without any restriction on $\Delta\phi$, i.e. for the whole ϕ interval $\Delta\phi = 180^{\circ}$) [1] are given there. Tables 1 and 2 correspond to the case ${P_t}^{clust} < 20\, GeV/c$ and serve as an illustration since it is rather a weak cut condition, while Tables 4 and 5 correspond to a more restrictive selection cut value $P_{tCUT}^{clust} = 5\, GeV/c$.

Firstly from the last summary lines of Tables 1–4 we can make a general conclusion about the $\Delta\phi$-dependence of the events spectrum. Thus, in the case of weak restriction

[1] The value $\Delta\phi = 5^{\circ}$ coincides with one CMS HCAL tower size in the ϕ-plane. and, thus, defines the precision of experimental registration of the jet $\vec{P_t}$ vector.

${P_t}^{clust} < 20\ GeV/c$ we can see from Table 1 that for the interval of $40 \leq {P_t}^{\gamma} \leq 50\,GeV/c$ there are about 66% of events concentrated in the $\Delta\phi < 15^{\circ}$ range, while 32% of events are in the $\Delta\phi < 5^{\circ}$ range. At the same time the analogous summary line of Table 2 shows us that at higher values $200 \leq {P_t}^{\gamma} \leq 240\,GeV/c$ the events spectrum moves to the small $\Delta\phi$ region: more than 99% of events have $\Delta\phi < 15^{\circ}$ and 79% of them have $\Delta\phi < 5^{\circ}$.

A tendency of very rapid concentration of the signal "$\gamma + Jet$" event distributions with the growth of ${P_t}^{\gamma}$ in a rather narrow back-to-back angle interval $\Delta\phi < 15^{\circ}$ becomes more distinctive with a more restrictive cut $P_{tCUT}^{clust} = 5\,GeV/c$ (see Tables 4 and 5). From the last summary line of the Tables 3 we see that in the case of $40 \leq {P_t}^{\gamma} \leq 50\,GeV/c$ more than 97% of the events have $\Delta\phi < 15^{\circ}$, while 68% of them are in the $\Delta\phi < 5^{\circ}$ range. At $200 \leq {P_t}^{\gamma} \leq 240\,GeV/c$ (see Table 5) more than 99% of the events that undergo this cut have $\Delta\phi < 5^{\circ}$. It means that imposing $P_{tCUT}^{clust} = 5\ GeV/c$ and suppressing cluster or mini-jet activity, we choose the events with a clean "back-to-back" (within 15°) topology of γ and jet orientation.

So, one can conclude that PYTHIA simulation predicts that at LHC energies most of the "$\gamma + Jet$" events after imposing $P_{tCUT}^{clust} = 20\,GeV/c$ may have the vectors $\vec{P}_t{}^{\gamma}$ and $\vec{P}_t{}^{jet}$ being back-to-back within $\Delta\phi < 15^{\circ}$. The cut $P_{tCUT}^{clust} = 5\ GeV/c$ improves this tendency [2].

It is worth mentioning that this picture reflects the predictions of one of the generators which are based on the approximate LO values for the cross section. It may change if the next-to-leading order or soft physics [3] effects are included and also after more real experimental data would be collected for comparison with a theory.

The other lines of the same Tables 1, 2 and 4, 5 contain the information about the P_t56 (see formula (3) of [1]) spectrum that in reality corresponds approximately, up to the fixed value of $\langle k_T \rangle = 0.44\ GeV/c$, to the ${P_t}^{ISR}$ spectrum.

From the comparison of Table 1 with Table 4 one can conclude that the most populated part of P_t56 (or ${P_t}^{ISR}$) spectrum reduces practically by twice with restricting P_{tCUT}^{clust}. So for $\Delta\phi_{max} = 15^{\circ}$ we see that it drops from $0 < P_t56 < 50\ GeV/c$ for $P_{tCUT}^{clust} = 20\ GeV/c$ to a more narrow interval of $0 < P_t56 < 20\,GeV/c$ for the $P_{tCUT}^{clust} = 5\,GeV/c$ case. At higher ${P_t}^{\gamma}$ interval for the same value $\Delta\phi_{max} = 15^{\circ}$ about the same factor 2 of P_t56 spectrum reduction (from an interval $0 < P_t56 < 50\ GeV/c$ for $P_{tCUT}^{clust} = 20\,GeV/c$ to a $0 < P_t56 < 20\ GeV/c$ for $P_{tCUT}^{clust} = 5\ GeV/c$) can be found from the comparison of Table 2 with Table 5.

From the same tables one can also see that P_t56 spectrum becomes slightly wider for higher values of ${P_t}^{\gamma}$: the dominant part of this spectrum in the interval $40 \leq {P_t}^{\gamma} \leq 50\ GeV/c$ spreads in the case of $P_{tCUT}^{clust} = 5\ GeV/c$ cut mainly within the interval $0 < P_t56 < 10\ GeV/c$ with the maximum peak at $0 < P_t56 < 5\ GeV/c$. At higher ${P_t}^{\gamma}$ interval $200 \leq {P_t}^{\gamma} \leq 240\ GeV/c$, P_t56 spectrum spreads out in a wider interval of $0 < P_t56 < 15\ GeV/c$ having the peak of its maximum at $5 < P_t56 < 10\ GeV/c$.

Thus, we can summarize that the PYTHIA generator used here predicts the values of ${P_t}^{ISR}$ spectrum to increase while growing ${P_t}^{\gamma}$, but its contribution can be reduced by imposing a restrictive cut on the value of ${P_t}^{clust}$ (for more details see Section 3 and the following papers [2, 3]).

[2] The enlarging of ${P_t}^{\gamma}$ values produces the same effect as it is seen from Tables 2 and 4 and will be demonstrated in more detail in our following papers [2, 3].

[3] We thank E. Pilon and J.Ph. Jouliet for the information about new FNAL data on this subject and on the importance of NLO corrections and soft physics effects.

Table 1: Number of events dependence on P_t56 and $\Delta\phi$ for $40 \leq Pt^{\gamma} \leq 50\,GeV/c$ and $P_{t_{CUT}}^{clust} = 20\,GeV/c$ for L_{int}=3fb^{-1}

P_t56 (GeV/c)	$\Delta\phi_{max}$			
	180°	15°	10°	5°
0 – 5	1103772	1049690	1006627	849706
5 – 10	1646004	1564393	1403529	812304
10 – 15	1331589	1122473	771060	380122
15 – 20	992374	568279	365329	179767
20 – 25	725537	282135	183406	91113
25 – 30	559350	169186	112308	58395
30 – 40	911942	265961	178048	89867
40 – 50	388950	94112	62068	31000
50 – 100	91248	19442	12973	6234
100 – 300	34	0	0	0
300 – 500	0	0	0	0
0 – 500	7750799	5135671	4095348	2498507

Table 2: Number of events dependence on P_t56 and $\Delta\phi$ for $200 \leq Pt^{\gamma} \leq 240\,GeV/c$ and $P_{t_{CUT}}^{clust} = 20\,GeV/c$ for L_{int}=3fb^{-1}

P_t56 (GeV/c)	$\Delta\phi_{max}$			
	180°	15°	10°	5°
0 – 5	1429	1429	1427	1380
5 – 10	3266	3266	3264	3150
10 – 15	3205	3205	3200	3069
15 – 20	2827	2827	2819	2618
20 – 25	2409	2408	2393	1918
25 – 30	2006	2006	1982	1300
30 – 40	2608	2605	2533	1411
40 – 50	1237	1230	1067	586
50 – 100	1066	1018	842	536
100 – 300	313	307	293	221
300 – 500	0	0	0	0
0 – 500	20366	20301	19820	16189

Table 3: Number of events dependence on $\Delta\phi_{max}$ and on $P_t{}^{\gamma}$ for $L_{int} = 3\,fb^{-1}$. $P_{t_{CUT}}^{clust} = 20\,GeV/c$ (summary)

$P_t{}^{\gamma}$ (GeV/c)	$\Delta\phi_{max}$			
	180°	15°	10°	5°
40 – 50	7750799	5135671	4095348	2498507
100 – 120	323766	297323	258691	176308
200 – 240	20366	20301	19820	16189
300 – 360	3638	3638	3627	3323

Table 4: Number of events dependence on P_t56 and $\Delta\phi$ for $40 \leq Pt^{\gamma} \leq 50\,GeV/c$ and $P_t^{clust}_{CUT} = 5\,GeV/c$ for L_{int}=3fb^{-1}

P_t56 (GeV/c)	$\Delta\phi_{max}$			
	180°	15°	10°	5°
0 – 5	331522	331321	329876	295759
5 – 10	319153	318581	299960	187089
10 – 15	88603	82586	60537	32335
15 – 20	21244	15327	11663	6924
20 – 25	8101	5681	4639	2992
25 – 30	4739	3395	2823	1949
30 – 40	3495	2790	2555	1714
40 – 50	1647	1277	1042	471
50 – 100	101	67	67	67
100 – 500	0	0	0	0
0 – 500	778606	761026	713161	529299

Table 5: Number of events dependence on P_t56 and $\Delta\phi$ for $200 \leq Pt^{\gamma} \leq 240\,GeV/c$ and $P_t^{clust}_{CUT} = 5\,GeV/c$ for L_{int}=3fb^{-1}

P_t56 (GeV/c)	$\Delta\phi_{max}$			
	180°	15°	10°	5°
0 - 5	369	369	369	369
5 - 10	563	563	563	562
10 - 15	217	217	217	217
15 - 20	56	56	56	56
20 - 25	20	20	20	18
25 - 30	9	9	9	7
30 - 40	7	7	7	6
40 - 50	6	6	6	5
50 - 100	10	10	10	10
100 - 300	8	8	8	8
300 - 500	0	0	0	0
0 - 500	1264	1264	1264	1257

Table 6: Number of events dependence on $\Delta\phi_{max}$ and on $P_t{}^{\gamma}$ for $L_{int} = 3\,fb^{-1}$. $P_t^{clust}_{CUT} = 5\,GeV/c$ (summary)

$P_t{}^{\gamma}$ (GeV/c)	$\Delta\phi_{max}$			
	180°	15°	10°	5°
40 – 50	778606	761026	713161	529299
100 – 120	22170	22143	22038	20786
200 – 240	1264	1264	1264	1257
300 – 360	212	212	212	212

Since the last lines in Tables 1, 2 and 4, 5 contain an important information on $\Delta\phi$ dependence of the total number of events, we supply these tables with the summarizing Tables 3 and 6. They include more intervals of ${P_t}^{\gamma}$ and contain analogous numbers of events that can be collected in different $\Delta\phi$ intervals for two different ${P_t}^{clust}$ cuts at $L_{int} = 3\,fb^{-1}$ (one month of LHC continuous running at low luminosity).

2.2 ${P_t}^{\gamma}$ and η^{γ} dependence of rates.

Since there are two main objects for experimental registration during the calibration procedure, namely a photon and a jet, we shall present here the number of events predicted by PYTHIA simulation with cuts defined by (1) for different intervals of ${P_t}^{\gamma}$ and η^{γ}. The lines of Table 7 correspond to ${P_t}^{\gamma}$-intervals while the columns — to η^{γ}-intervals . The last column of this table contains the total number of events in the whole ECAL (at $L_{int} = 3\,fb^{-1}$) η^{γ}-region $0 < |\eta^{\gamma}| < 2.61$ for a given ${P_t}^{\gamma}$-interval. We see from here that the events number decreases fastly with the ${P_t}^{\gamma}$ growth (by more than 50% for each following interval) while for the fixed ${P_t}^{\gamma}$- interval there are no big changes with the variation of η^{γ}. Since $L_{int} = 3\,fb^{-1}$ corresponds approximately to one month of LHC continuous running, we conclude that these rates demonstrate that, in principle, there would

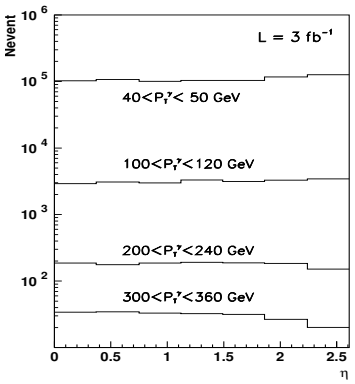

Fig. 1: η-dependence of rates for different ${P_t}^{\gamma}$-intervals

Table 7: Rates for $L_{int} = 3\,fb^{-1}$ for different intervals of ${P_t}^{\gamma}$ and η^{γ} ($P_{t\,CUT}^{clust} = 5\,GeV/c$ and $\Delta\phi \leq 15^{\circ}$).

${P_t}^{\gamma}$	η^{γ} intervals							all η^{γ}
(GeV/c)	0.0-0.4	0.4-0.7	0.7-1.1	1.1-1.5	1.5-1.9	1.9-2.2	2.2-2.6	0.0-2.6
40 – 50	102656	107148	100668	103903	103499	116674	126546	761027
50 – 60	43905	41729	41074	45085	42974	47640	50310	312697
60 – 70	18153	18326	19190	20435	20816	19432	23650	140005
70 – 80	9848	10211	9963	10166	9951	11397	10447	71984
80 – 90	5287	5921	5104	5823	5385	6067	5923	39509
90 – 100	2899	3033	3033	3326	3119	3265	3558	22234
100 – 120	2908	3091	2995	3305	3133	3282	3429	22143
120 – 140	1336	1359	1189	1346	1326	1499	1471	9525
140 – 160	624	643	626	674	706	614	668	4555
160 – 200	561	469	557	555	519	555	557	3774
200 – 240	187	176	186	192	187	185	151	1264
240 – 300	103	98	98	98	100	92	74	665
300 – 360	34	34	33	32	31	27	20	212
40 – 360	188517	192274	184734	194957	191761	210742	226819	1389484

be quite enough number of events for the jet mass scale setting and successful calibration of HCAL. Fig. 1 gives a compact illustration of rates for four ${P_t}^{\gamma}$-intervals, considered here,

completely contained in these regions, while column HE+HF gives the number of the events where the jet covers both the HE and HF regions. From these tables we can see what number

and it shows a very weak dependence on η^{γ} (or better to speak about their independence on η^{γ}).

2.3 Estimation of "$\gamma + Jet$" events rates for HB, HE and HF regions.

Since the jet is a wide spread object, the η^{jet} dependence of rates for different ${P_t}^{\gamma}$-intervals will be presented in a different way than in Table 7. Namely, Tables 8–11 include the rates of events for different η^{jet} intervals, covered by the barrel, endcap and forward (HB, HE and HF) parts of HCAL and for different ${P_t}^{Jet}$ intervals (for a case of $L_{int} = 3\, fb^{-1}$). The selection cuts are taken as those of Section 3.2 of [1] specified by the following values of cuts parameters:

Table 8: Selection 1. $\Delta {P_t}^{jet}/{P_t}^{jet} = 0.00$

${P_t}^{\gamma}$	HB	HB+HE	HE	HE+HF	HF
40 – 50	260259	211356	141759	102299	45354
50 – 60	108827	89126	55975	41553	17216
60 – 70	49585	40076	25172	18153	7019
70 – 80	25506	20897	12881	9679	3021
80 – 90	14083	11720	7529	4873	1304
90 – 100	7261	7054	4142	2924	853
100 – 120	7703	6913	4013	2926	588
120 – 140	3372	2977	1805	1164	207
140 – 160	1650	1481	865	509	50
160 – 200	1493	1137	708	396	40
200 – 240	503	406	242	107	6
240 – 300	287	215	122	40	1
300 – 360	96	73	35	8	0
40 – 360	480538	393378	255266	184642	75660

Table 9: Selection 1. $\Delta {P_t}^{jet}/{P_t}^{jet} \leq 0.10$

${P_t}^{\gamma}$	HB	HB+HE	HE	HE+HF	HF
40 – 50	341043	55160	263629	26653	74534
50 – 60	144955	20396	108765	9300	29281
60 – 70	65525	8541	49412	3907	12621
70 – 80	34155	4093	25918	1957	5860
80 – 90	19224	1961	14741	804	2778
90 – 100	10258	1304	8394	536	1742
100 – 120	10859	1043	8357	545	1338
120 – 140	4618	509	3675	178	546
140 – 160	2325	222	1751	90	168
160 – 200	1971	147	1458	52	147
200 – 240	685	61	472	20	26
240 – 300	383	32	234	7	9
300 – 360	129	10	72	1	0
40 – 360	636418	93480	486788	44052	129050

$$P_{tCUT}^{isol} = 5\ GeV/c; \quad \epsilon_{CUT}^{\gamma} = 7\%; \quad \Delta\phi < 15^{\circ}; \quad P_{tCUT}^{clust} = 5\ GeV/c. \tag{2}$$

No any restrictions on other parameters are used. The first columns of these tables give the number of events with jets (found by LUCELL jetfinding algorithm of PYTHIA), all particles of which are comprised completely (100%) in the barrel part (HB) and there is a 0% sharing of ${P_t}^{jet}$ (${\Delta P_t}^{jet}$) between HB and neighbouring HE part of HCAL, i.e. ${\Delta P_t}^{jet} = 0$. Second columns of these tables contain a number of the events in which P_t of the jet is shared between HB and HE regions. The same sequence of restriction conditions takes place in the following columns. Thus, HE and HF columns include a number of events with the jets

Table 10: Selection 2. ${\Delta P_t}^{jet}/{P_t}^{jet} = 0.00$

${P_t}^{\gamma}$	HB	HB+HE	HE	HE+HF	HF
40 – 50	46972	32954	26114	16208	10041
50 – 60	23717	18911	13448	8367	5047
60 – 70	14384	9751	7469	4703	2386
70 – 80	8546	6733	4627	2960	1206
80 – 90	5653	4386	3107	1925	573
90 – 100	3326	3119	1900	1377	390
100 – 120	4157	3435	2271	1467	324
120 – 140	2183	1786	1185	710	134
140 – 160	1175	1005	635	362	31
160 – 200	1179	905	565	314	25
200 – 240	442	353	212	97	5
240 – 300	273	200	116	37	1
300 – 360	94	71	35	7	0
40 – 360	112111	83617	61686	38535	20163

Table 11: Selection 2. ${\Delta P_t}^{jet}/{P_t}^{jet} \leq 0.10$

${P_t}^{\gamma}$	HB	HB+HE	HE	HE+HF	HF
40 – 50	60113	7986	45388	3909	14894
50 – 60	31495	3631	25134	1971	7259
60 – 70	18326	2248	13139	968	4011
70 – 80	11385	1243	8741	573	2132
80 – 90	7614	633	5957	292	1145
90 – 100	4544	536	3886	280	865
100 – 120	5771	481	4434	278	689
120 – 140	2909	272	2370	94	352
140 – 160	1648	138	1246	65	111
160 – 200	1560	113	1162	38	115
200 – 240	600	53	416	17	23
240 – 300	362	30	220	6	8
300 – 360	126	10	71	1	0
40 – 360	146468	17374	112177	8492	31603

of the events can, in principle, be suitable for the most precise calibration procedure, carried out separately for HB, HE and HF parts of HCAL in different intervals of ${P_t}^{jet}$.

Less restrictive conditions, when up to 10% of the jet P_t are allowed to be shared between HB, HE and HF parts of HCAL, are given in Tables 9 and 11. Tables 8 and 9 correspond to the case of Selection 1 (see [1]). Tables 10 and 11 contain a number of events collected with addition of Selection 2 restriction, i.e. they include only the events with "isolated jets" (whose definition is given by (26) in the same Section 3.2 of [1]).

From Table 8, that corresponds to the most restrictive selection and gives the number of events most suitable for HCAL calibration, we see from the last summarizing lines that for the interval $40 < Pt^{\gamma} < 360\ GeV/c$ PYTHIA predicts around a half of million of events for HB and a quarter of million of events for HE per one month of continuous data taking at low LHC luminosity, while for HF it is expected to be less than 80 000 events per month.

One should keep in mind that the last columns in Tables 8–11 can not be taken as the final result here as we have not defined the meaning of sharing ${P_t}^{jet}$ between the HF regions and the region with $|\eta| > 5$, i.e. close to a "beam-pipe" region. A more accurate estimation can be done here by finding events with jets in a wider region than the HF volume restricted by $3 < |\eta^{HF}| < 5$ and by calculation of a number of those events whose jets are contained in HF completely with all particles belonging to them.

3. STUDY OF FEATURES OF "$\gamma + Jet$" EVENTS IN THE HCAL BARREL REGION.

In this section we shall study a specific sample of events that may be most suitable for HB calibration. It is a sample of events in which jets are completely (100%) contained in HB region, i.e. having 0% sharing of ${P_t}^{jet}$ (at PYTHIA level of simulation) with HE. Below we shall call them "HB-events". A particular set of these events for ${P_t}^{clust} = 5\ GeV/c$ is presented in the first column (HB) of Table 8. Here we shall use two different jetfinders, namely, LUCELL from PYTHIA and UA1 (the last one is taken [4] from CMSJET [6]) for an equal foot determination of clusters and jets. The distributions of ${P_t}^{clust}$ for generated events found by these two different jetfinders in two ${P_t}^{\gamma}$ intervals, $40 < {P_t}^{\gamma} < 50 GeV/c$ and $300 < {P_t}^{\gamma} < 360 GeV/c$, are shown in Fig. 2 for $P_{tCUT}^{clust} = 30\ GeV/c$.

3.1 Influence of the P_{tCUT}^{clust} parameter on the photon and jet P_t balance and initial state radiation suppression.

Here we shall study correlation of ${P_t}^{clust}$ with ${P_t}^{ISR}$ proportional to $P_t 56$ for the fixed $\langle k_T \rangle$ (The influence of the $\langle k_T \rangle$ variation on the ${P_t}^{\gamma}$ and ${P_t}^{Jet}$ balance is discussed in [4]).

The banks of 1-jet "$\gamma + Jet$" events gained from the already mentioned (in Section 2.1) results of PYTHIA generation of 10^7 signal "$\gamma + Jet$" events in each of four ${P_t}^{\gamma}$ intervals (40 – 50, 100 – 120, 200 – 240, 300 – 360 GeV/c) will be used here. The observables defined in Sections 3.1 and 3.2 of paper [1] will be restricted here by Selection 1 cuts (17) – (24) of Section 3.2 of [1] and the cut parameters defined by (1). The luminosity was chosen to be $L = 10^{33}\, cm^2 sec^{-1}$.

[4] In order to select events with ${P_t}^{clust}$ value starting from $5\ GeV/c$ we have changed the P_t precluster threshold in the UA1 algorithm from 10 GeV/c, taken as default value, to 1.5 GeV/c . We also increase the cone radius in the UA1 algorithm from 0.5 to 0.7.

We have chosen two of these intervals with the extreme values of $P_t{}^{\gamma}$ to illustrate the influence of the P_{tCUT}^{clust} parameter on the distributions of physical variables. The results of

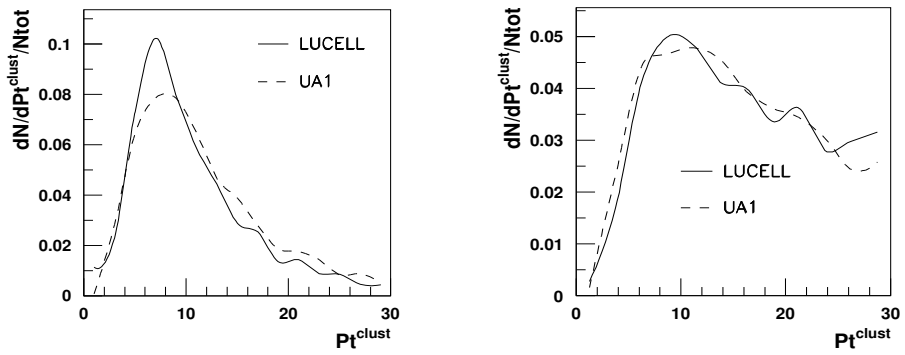

Fig. 2: $P_t{}^{clust}$-distribution in "$\gamma + Jet$" events from two $P_t{}^{\gamma}$ intervals: a) $40 < P_t{}^{\gamma} < 50\,GeV/c$ and b) $300 < P_t{}^{\gamma} < 360\,GeV/c$ with the same cut $P_{tCUT}^{clust} = 30\ GeV/c$.

P_{tCUT}^{clust} variation are shown in Fig. 3 for $40 < P_t{}^{\gamma} < 50\ GeV/c$ and in Fig. 4 for $300 < P_t{}^{\gamma} < 360\ GeV/c$. In these figures, in addition to three variables P_t56, $P_t{}^{\eta>5}$, $P_t{}^{out}$, already explained in Sections 2.2, 3.1 and 3.2 of [1], we present the distributions for other two variables, $P_t(O{+}\eta > 5)$ and $(1 - cos\Delta\phi)$, which define the right-hand side of equation (29) of [1]. The distribution for the back-to-back $\Delta\phi$ angle (see (23) of [1]) which defines the second variable, is also presented in Figs. 3, 4.

The disbalance variable P_t56 (defined by formula (3) of [1]) and both components of another disbalance measure $(P_t{}^{\gamma} - P_t{}^{jet})/P_t{}^{\gamma}$ (defined by formula (29) of [1]) as a sum of $(1 - cos\Delta\phi)$ and $P_t(O{+}\eta > 5)$, as well as two others, $P_t{}^{out}$ and $\Delta\phi$, show a tendency, as it is seen from Figs. 3 and 4, to become smaller with the restriction of the upper limit on the $P_t{}^{clust}$ value. It means that the calibration precision may increase with decreasing P_{tCUT}^{clust}, which justifies the intuitive choice of this new variable in Section 3 of [1]. The origin of this improvement becomes clear from the P_t56 density plot, which demonstrates suppression of P_t56 (or $P_t{}^{ISR}$) with implying a more restrictive cut on $P_t{}^{clust}$.

The comparison of Fig. 3 (for $40 < P_t{}^{\gamma} < 50\ GeV/c$) and Fig. 4 (for $300 < P_t{}^{\gamma} < 360\ GeV/c$) shows that a degree of back-to-backness of the photon and jet P_t vectors in the ϕ-plane increases with increasing $P_t{}^{\gamma}$. At the same time $P_t{}^{out}$ and $P_t{}^{ISR}$ distributions become wider, while the $P_t{}^{\eta>5}$ distribution practically does not depend on $P_t{}^{\gamma}$ and $P_t{}^{clust}$.

It should be mentioned that the results presented in Figs. 3 and 4 were obtained with the LUCELL jetfinder of PYTHIA [5].

[5] The results obtained with both jetfinders and $P_t{}^{\gamma}$ and $P_t{}^{Jet}$ balance will be discussed in [2, 3] in more detail

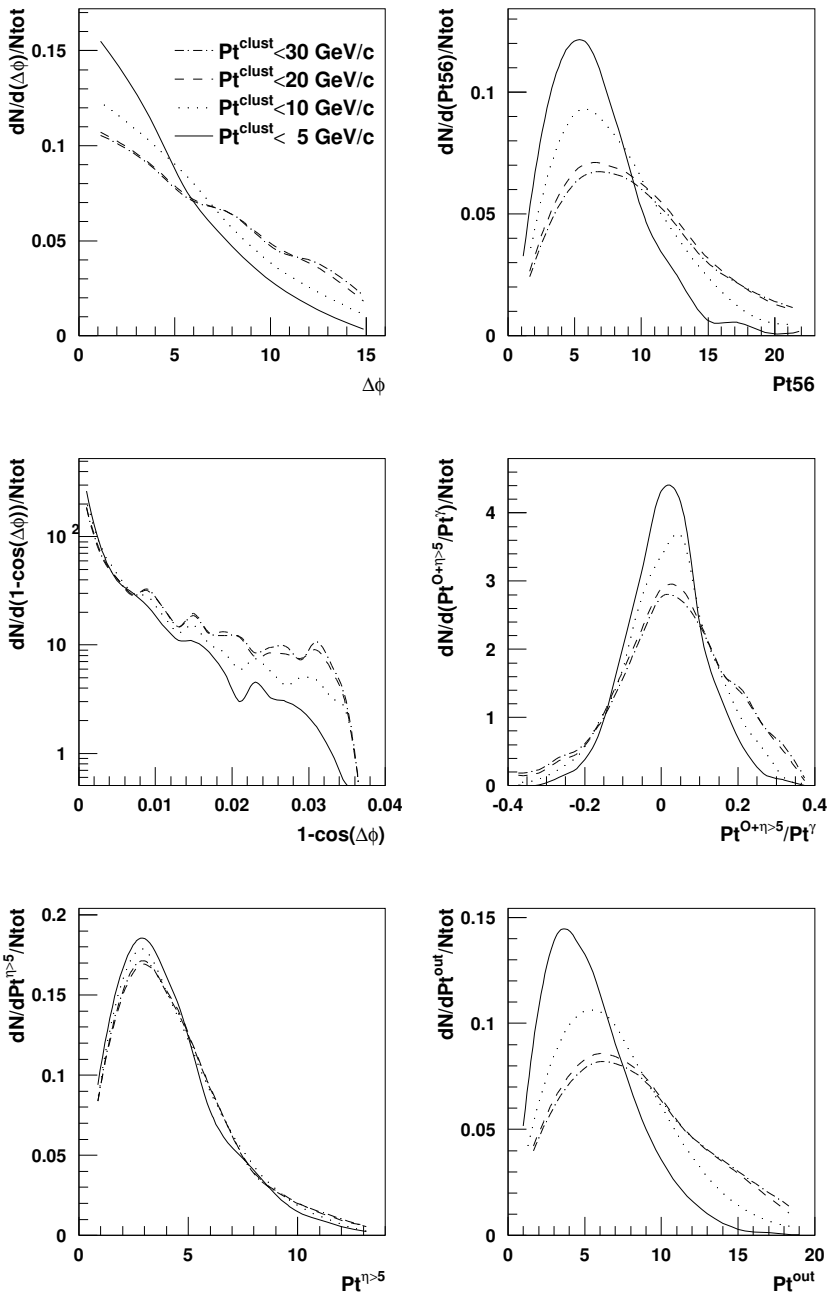

Fig. 3: LUCELL algorithm, $\Delta\phi < 15^\circ$, $40 < {P_t}^\gamma < 50\, GeV/c$. Selection 1.

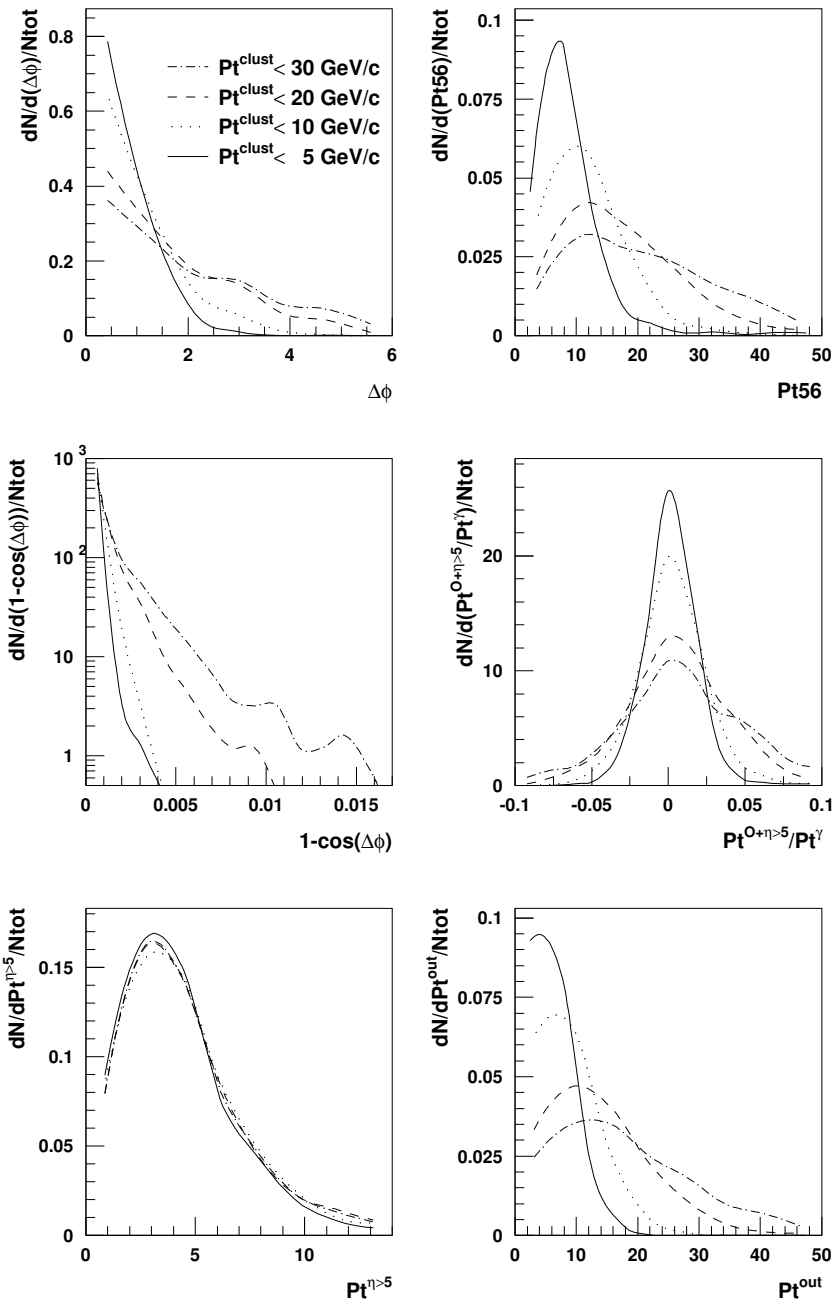

Fig. 4: LUCELL algorithm, $\Delta\phi < 15°$, $300 < {P_t}^{\gamma} < 360\, GeV/c$. Selection 1.

3.2 Jetfinders and P_t structure of jets in $\eta - \phi$ space.

In order to understand well the calibration procedure of "$\gamma + Jet$" events, it is useful to keep control over some principal characteristics of jets and of the P_t activity in the space around them. The left-hand columns of Figs. 5 and 6 represent jet radius $R^{jet}(\eta, \phi)$ distributions in these HB-events for the intervals: $40 < {P_t}^{\gamma} < 50\, GeV/c$ and $300 < {P_t}^{\gamma} < 360\, GeV/c$, respectively. We have chosen the jet radius counted from the initiator cell (ic) to be restricted by $R_{ic}^{jet} = 0.7$ for the LUCELL and UA1 jetfinders.

From the left-hand side plots in Figs. 5 and 6 we see that both jetfinders give close enough results for R_{gc}^{jet} distribution. In these plots the radius in $\eta - \phi$ space is counted from the gravity center (gc). The detailed information about averaged values of the jet radius for four ${P_t}^{\gamma}$-intervals will be presented in the tables of Appendices 1–4 of [3] [6].

Let us now consider the question, how the transverse momentum is distributed inside a jet. Let us divide the jet radius $R^{jet}(\eta, \phi) \equiv R$ into a set of ΔR bins and calculate the vector sums of cells P_t in each ΔR_{bin} ring. Normalized to ${P_t}^{Jet}$, the modulus of this vector sum, denoted by ${P_t}^{bin}$, would give the value that tells us what portion of ${P_t}^{Jet}$ is contained in the ring of size ΔR_{bin}. Its variation with the distance R counted from the center of gravity of the jet is shown in the right-hand columns of Figs. 5 and 6.

From these figures we can conclude that the LUCELL and UA1 jetfinders lead to equally P_t-densed central part inside the jet.

3.3 P_t distribution inside and outside a jet.

Now let us see how the volume outside the jet, (i.e. calorimeter cells outside the jet cone), may be populated by P_t in these HB "$\gamma + Jet$" events. For this purpose we calculate a vector sum $\vec{P}_t^{\,sum}$ of individual transverse momenta of $\Delta\eta \times \Delta\phi$ cells, included by a jetfinder into a jet as well as of cells in a larger volume that surrounds a jet. In the last case this procedure in some sense can be viewed as some straightforward enlarging of the jet radius in the $\eta - \phi$ space.

The figures that represent the ratio ${P_t}^{sum}/{P_t}^{\gamma}$, as a function of the distance $R(\eta, \phi)$ counted from the jet gravity center towards its boundary and further into space outside the jet are shown in the left-hand columns of Figs. 7 and 8 for a case when all jet particles are kept in the jet, while the case of the magnetic field effect account (i.e. when the contribution from charged particles with $P_t \leq 0.8\ GeV/c$ is removed [7] from the total jet P_t in a case of HB events) is shown in the left-hand columns of Figs. 9 and 10.

From these figures we see that the jet surrounding space is found to be far from being an empty one in the case of "$\gamma + Jet$" events considered here. We also see that an average value of the total ${P_t}^{sum}$ increases with increasing the volume around the jet and it exceeds ${P_t}^{\gamma}$ at $R = 0.7 - 0.8$ when all particles are included into the jet (see Figs. 7 and 8), while in the case of rejected charged particles with ${P_t}^{ch} < 0.8\ GeV/c$ only about $95 - 97\%$ of ${P_t}^{Jet}$ are collected at $R = 0.7 - 0.8$.

From the right-hand column of Fig. 7 we see that when all particles are included into the jet, the following disbalance measure:

[6] From there one can see a weak dependence of the jet radius on ${P_t}^{Jet} (\approx {P_t}^{\gamma})$ for both UA1 and LUCELL algorithms

[7] See [5]

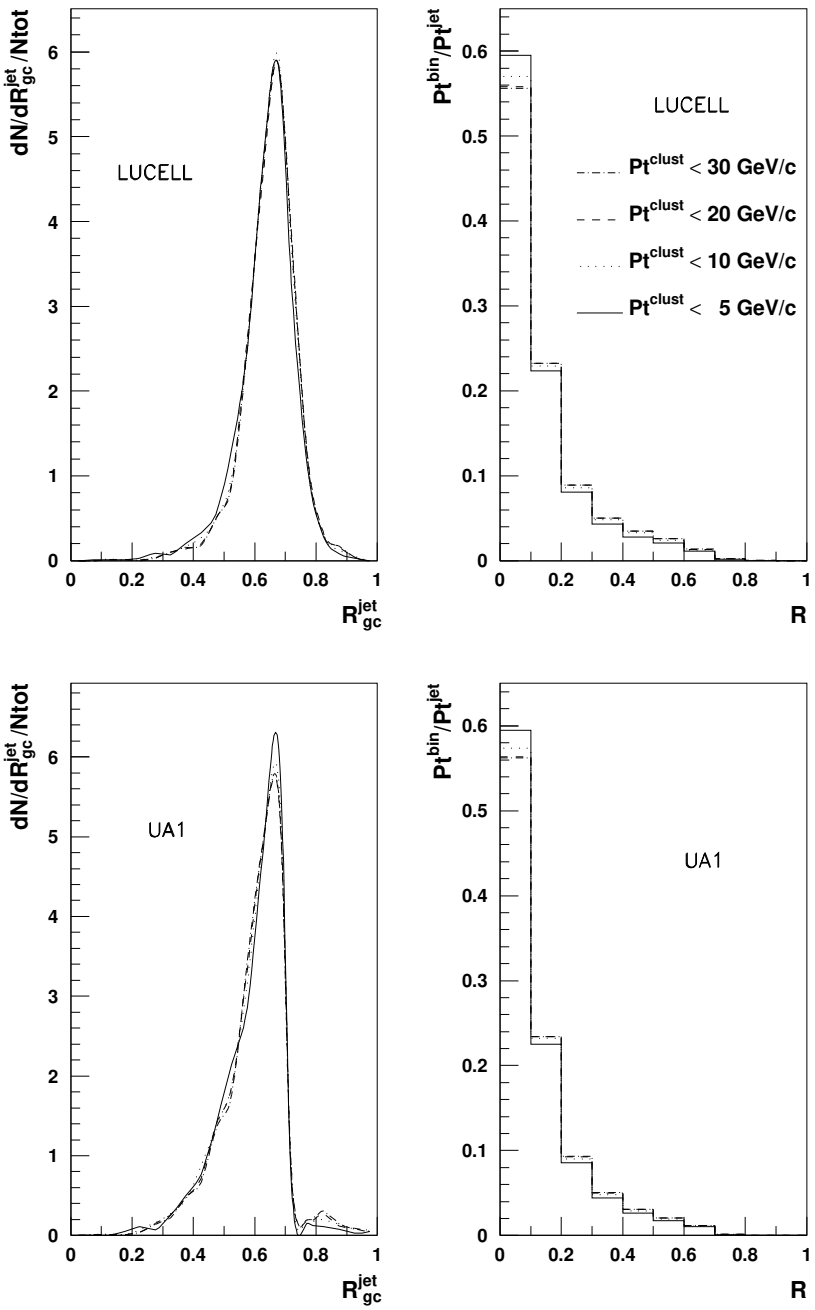

Fig. 5: LUCELL and UA1 algorithms, $\Delta\phi < 15°$, $40 < P_t{}^{\gamma} < 50\,GeV/c$. Selection 1.

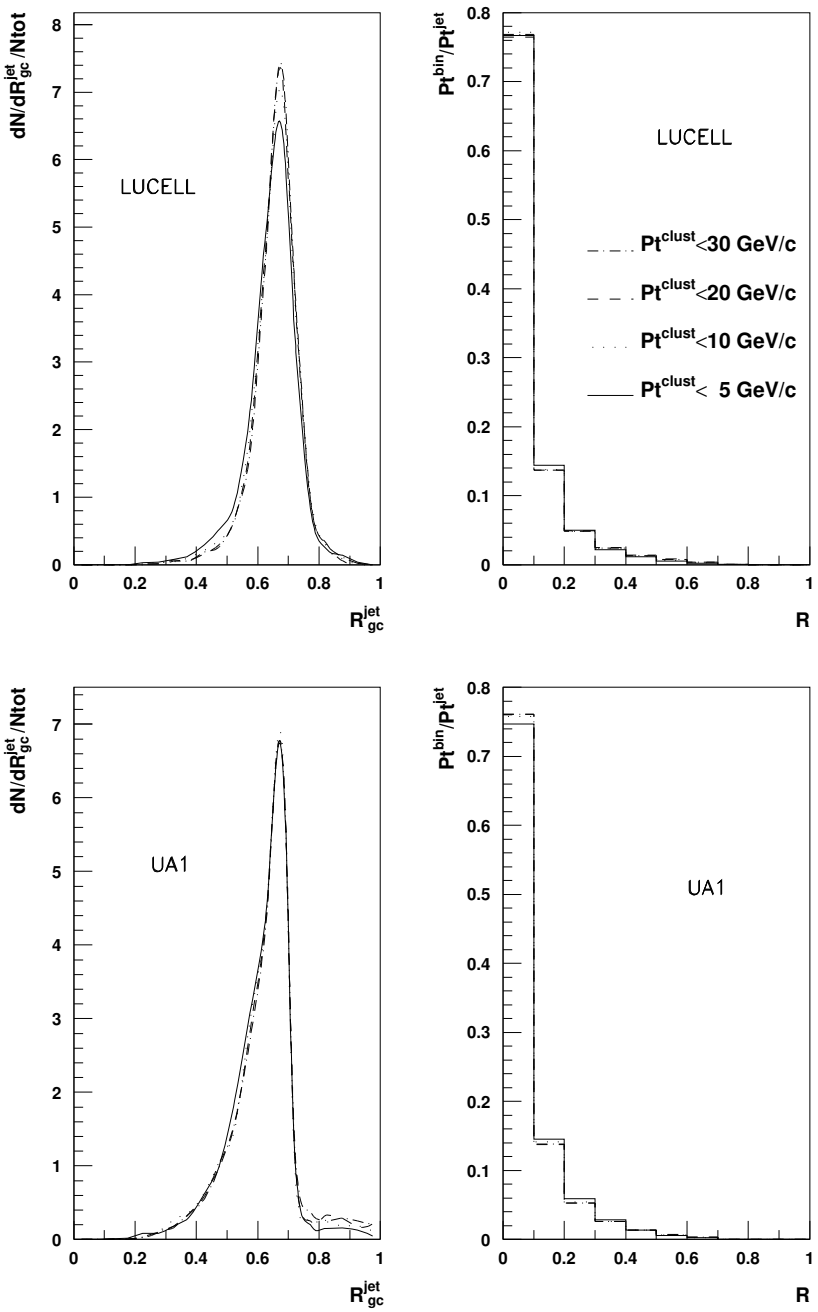

Fig. 6: LUCELL and UA1 algorithms, $\Delta\phi < 15°$, $300 < P_t{}^{\gamma} < 360\, GeV/c$. Selection 1.

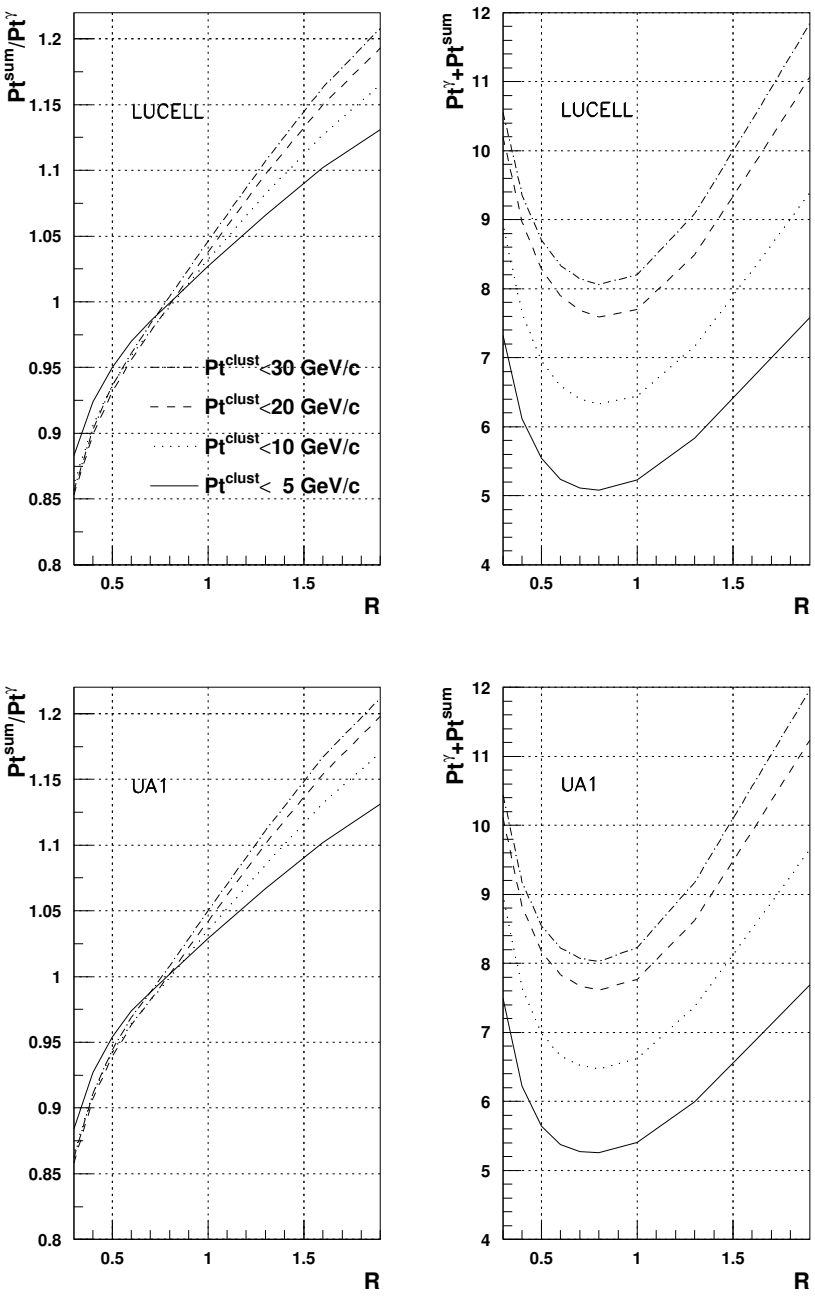

Fig. 7: LUCELL and UA1 algorithms, $\Delta\phi < 15°, 40 < P_t{}^{\gamma} < 50\, GeV/c$

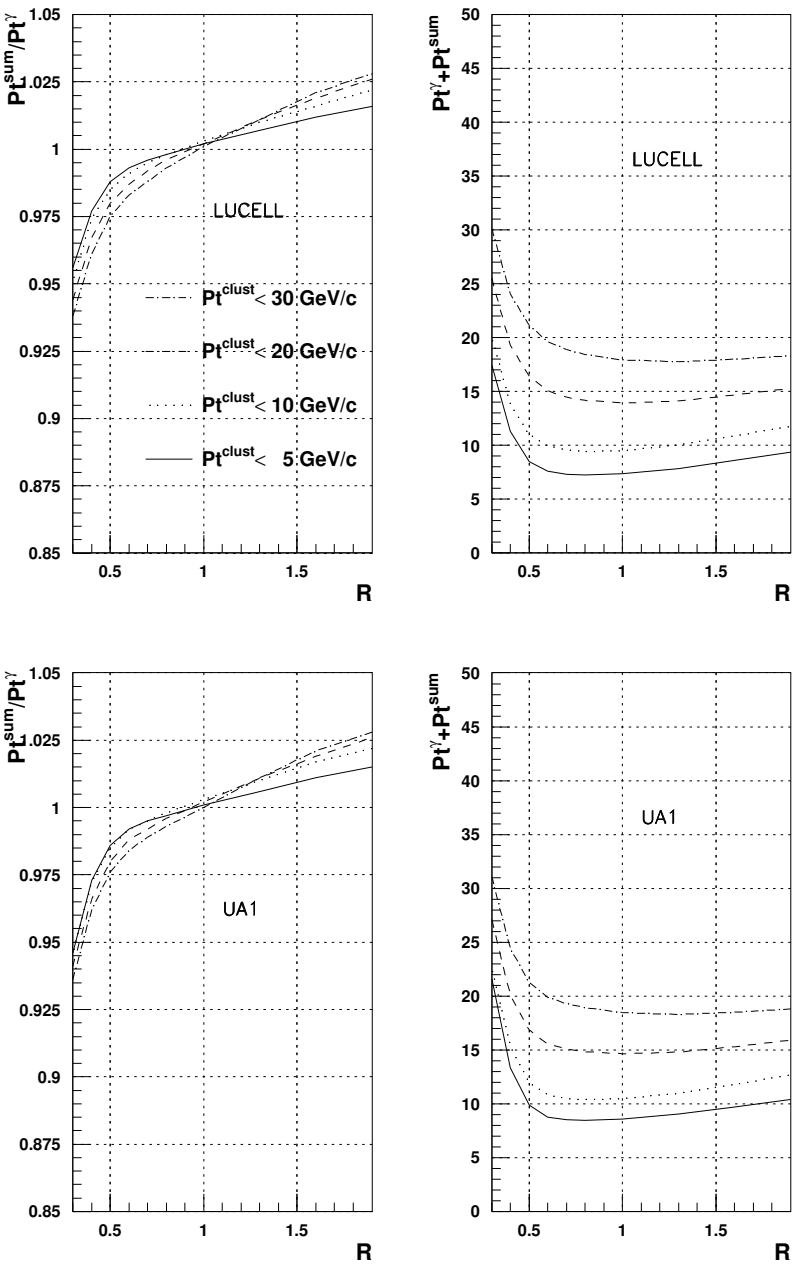

Fig. 8: LUCELL and UA1 algorithms, $\Delta\phi < 15°$, $300 < P_t{}^{\gamma} < 360\, GeV/c$

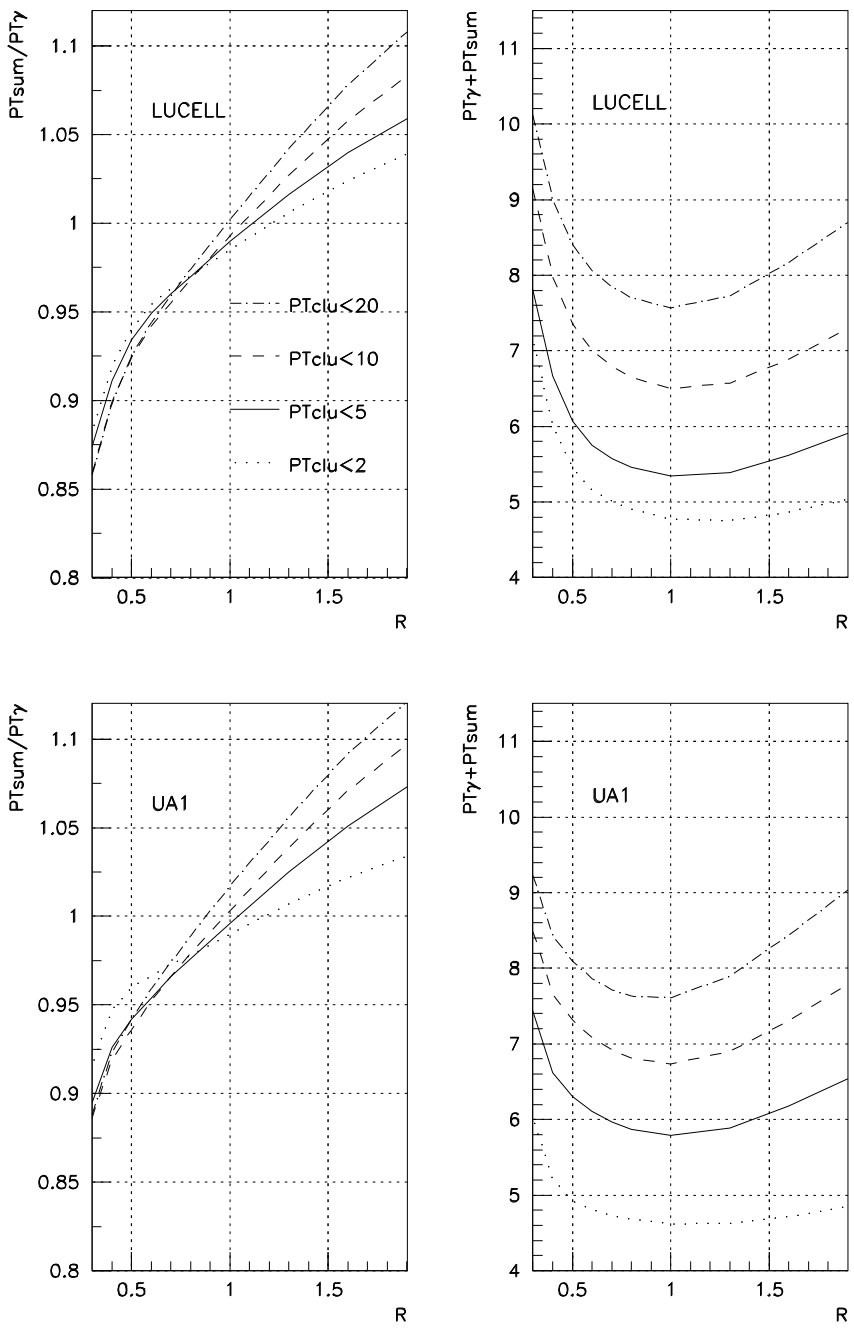

Fig. 9: LUCELL and UA1 algorithms, $\Delta\phi < 15°,\ 40 < P_t{}^{\gamma} < 50\ GeV/c,\ P_{t_{ch}}^{jet} > 0.8\ GeV/c$.

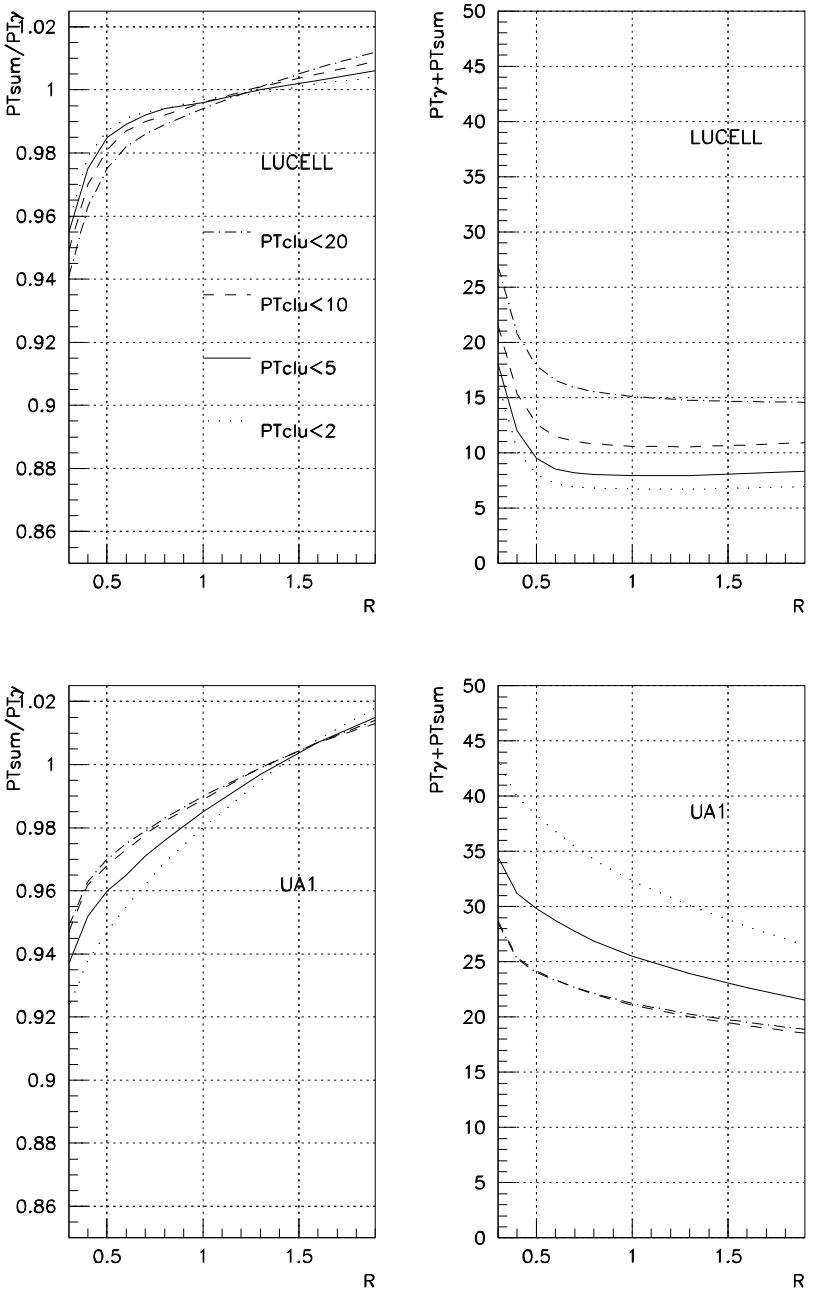

Fig. 10: LUCELL and UA1 algorithms, $\Delta\phi < 15°,\ 300 < P_t{}^{\gamma} < 360\ GeV/c,\ P_{t_{ch}}^{jet} > 0.8\ GeV/c$.

$$P_t{}^{\gamma+sum} = \left|\vec{P}_t{}^{\gamma} + \vec{P}_t{}^{sum}\right| \quad (3)$$

achieves its minimum at $R \approx 0.7 - 0.8$ for both LUCELL and UA1 algorithms. From Figs. 9 and 10 we see that with account of the magnetic field effect on charged particles with $P_t{}^{ch} < 0.8\ GeV/c$ the minimum of $P_t{}^{\gamma+sum}$ is achieved at larger values of $R \approx 1.0$ again for both LUCELL and UA1 jetfinders.

The value of $P_t{}^{\gamma+sum}$ continues to grow rapidly with increasing R after the point R=1 for $40 < P_t{}^{\gamma} < 50\ GeV/c$ (see Figs. 7, 9), while for higher $P_t{}^{\gamma}$ (see Figs. 8, 10 for the $300 < P_t{}^{\gamma} < 360\ GeV/c$ interval) the ratio $P_t{}^{sum}/P_t{}^{\gamma}$ and the disbalance measure $P_t{}^{\gamma+sum}$ increase more slowly with increasing R after the point R=0.7. This means that at higher $P_t{}^{\gamma}$ (or $P_t{}^{Jet}$) the topology of "$\gamma + Jet$" events becomes more pronounced and we get a cleaner picture of an "isolated" jet. This feature clarifies the motivation of introduction of two criteria "Selection 2", (see "Point 8") and of "Selection 3" (see "Point 9") in Section 3.2 of [1] for selection of events with "isolated jets".

4. SUMMARY

From the study in Section 2.1 we see that the PYTHIA simulation predicts that most "$\gamma + Jet$" events at LHC energies may have the vectors $\vec{P}_t{}^{\gamma}$ and $\vec{P}_t{}^{Jet}$ being back-to-back within $\Delta\phi < 15^{\circ}$ (about 66% for $40 \le P_t{}^{\gamma} \le 50\ GeV/c$ and greater than 99% for $P_t{}^{\gamma} \ge 200\ GeV/c$). At the same time, as it is seen from Table 1, a substantial part of the $P_t{}^{ISR}(\approx P_t56)$ spectrum spreads out in the interval $0 < P_t56 < 20\ GeV/c$, having the peak inside the $5 < P_t56 < 10\ GeV/c$ interval and noticeable tails (about of $5 - 10\%$ of number of events) extending to $P_t56 = 40\ GeV/c$ not only for $\Delta\phi < 15^{\circ}$ but also for the smaller $\Delta\phi < 10^{\circ}$ and $\Delta\phi < 5^{\circ}$ intervals. From here we can conclude that the use of only one traditional $\Delta\phi$ cut does not help much to reduce the $P_t{}^{ISR}$ contribution at LHC energies. It is most obvious from Table 2, where we find that at high $P_t{}^{\gamma}$ ($200 < P_t{}^{\gamma} < 240\ GeV/c$) more that 99% of events belong to the $\Delta\phi < 15^{\circ}$ interval. Most of these events lay within the $0 < P_t56 < 50\ GeV/c$ interval. Even for $\Delta\phi < 5^{\circ}$, a considerable part of the spectrum belongs to the interval $0 < P_t56 < 40\ GeV/c$. Thus, a decrease in $\Delta\phi$ has, in fact, no big influence on the $P_t{}^{ISR}$ spectrum and it cannot be useful to reduce the number of events with essential amount of initial state radiation at LHC energies.

In Section 3 the efficiency of P_{tCUT}^{clust} for ISR suppression was demonstrated. From Figs. 3 and 4 we see that the distribution for P_t56 becomes narrower with decreasing P_{tCUT}^{clust}. Analogous behavior is shown by the $P_t{}^{out}$ (as $P_t{}^{clust}$ is a part of $P_t{}^{out}$) spectra. These figures serve as an illustration for a more detailed study of P_{tCUT}^{clust} influence on $P_t{}^{\gamma}$ and $P_t{}^{Jet}$ balance, which will be presented in our next papers [2–4].

A strict limitation of the P_{tCUT}^{clust} parameter, introduced in Section 3.2 of [1], (by $\approx 5 - 10\ GeV/c$) improves this tendency. Simultaneously, due to this limitation, one can noticeably reduce radiation in the initial state (compare Tables 1, 4 and 2, 5), which leads to decreasing $P_t{}^{\gamma}$ and $P_t{}^{Jet}$ disbalance.

From Section 2.3 (Table 8) we see that even with the restrictive cuts mentioned there one can expect around a half million of events for HB, a quarter million of events for HE, and less than 80 000 events for the HF part and $L_{int} = 3\ fb^{-1}$ (i.e. per month of continuous data taking at low LHC luminosity) for interval $40 < Pt^{\gamma} < 360\ GeV/c$ for the sample of events that corresponds to $0\%\ P_t$ sharing between HCAL parts. Despite those cuts the number of

events for the HCAL part above, in principle, can be quite sufficient for successful jet energy scale setting and HCAL calibration.

5. ACKNOWLEDGEMENTS

We are greatly thankful to D. Denegri for having offered this theme to study, fruitful discussions and permanent support and encouragement. It is a pleasure for us to express our recognition for helpful discussions to P. Aurenche, M. Dittmar, M. Fontannaz, J.Ph. Guillet, M.L. Mangano, E. Pilon, H. Rohringer, S. Tapprogge and J. Womersley.

References

[1] D.V. Bandourin, V.F. Konoplyanikov, N.B. Skachkov. "Jet energy scale setting with "$\gamma + Jet$" events at LHC energies. Generalities, selection rules". JINR Communication, JINR, Dubna, 2000-

[2] D.V. Bandourin, V.F. Konoplyanikov, N.B. Skachkov. "Jet energy scale setting with "$\gamma + Jet$" events at LHC energies. Minijets and cluster suppression and ${P_t}^{\gamma} - {P_t}^{Jet}$ disbalance". JINR Communication, JINR, Dubna, 2000-

[3] D.V. Bandourin, V.F. Konoplyanikov, N.B. Skachkov. "Jet energy scale setting with "$\gamma + Jet$" events at LHC energies. Selection of events with a clean "$\gamma + Jet$" topology and ${P_t}^{\gamma} - {P_t}^{Jet}$ disbalance". JINR Communication, JINR, Dubna, 2000-

[4] D.V. Bandourin, V.F. Konoplyanikov, N.B. Skachkov. "Jet energy scale setting with "$\gamma + Jet$" events at LHC energies. Detailed study of the background suppression". JINR Communication, JINR, Dubna, 2000-

[5] CMS Tracker project, Technical Design Report, CERN/LHCC 98–6, CMS TDR 5, p. 467.

[6] S. Abdullin, A. Khanov, N. Stepanov, CMS Note CMS TN/94–180 "CMSJET".